



# CHORUS

This is the accepted manuscript made available via CHORUS. The article has been published as:

## Nonuniform Flow Dynamics Probed by Nanosecond X-Ray Speckle Visibility Spectroscopy

Yanwen Sun, Gabriella Carini, Matthieu Chollet, Franz-Josef Decker, Mike Dunne, Paul Fuoss, Stephan O. Hruszkewycz, Thomas J. Lane, Kazutaka Nakahara, Silke Nelson, Aymeric Robert, Takahiro Sato, Sanghoon Song, G. Brian Stephenson, Mark Sutton, Tim B. Van Driel, Clemens Weninger, and Diling Zhu

Phys. Rev. Lett. **127**, 058001 — Published 28 July 2021

DOI: [10.1103/PhysRevLett.127.058001](https://doi.org/10.1103/PhysRevLett.127.058001)

# Non-uniform flow dynamics probed by nanosecond x-ray speckle visibility spectroscopy

Yanwen Sun,<sup>1</sup> Gabriella Carini,<sup>1,\*</sup> Matthieu Chollet,<sup>1</sup> Franz-Josef Decker,<sup>1</sup> Mike Dunne,<sup>1</sup> Paul Fuoss,<sup>1</sup> Stephan O. Hruszkewycz,<sup>2</sup> Thomas J. Lane,<sup>1</sup> Kazutaka Nakahara,<sup>1</sup> Silke Nelson,<sup>1</sup> Aymeric Robert,<sup>1</sup> Takahiro Sato,<sup>1</sup> Sanghoon Song,<sup>1</sup> G. Brian Stephenson,<sup>2</sup> Mark Sutton,<sup>3,1</sup> Tim B. Van Driel,<sup>1</sup> Clemens Weninger,<sup>1,†</sup> and Diling Zhu<sup>1,‡</sup>

<sup>1</sup>*Linac Coherent Light Source, SLAC National Accelerator Laboratory, Menlo Park, California, 94025, USA*

<sup>2</sup>*Materials Science Division, Argonne National Laboratory, Lemont, 60439, U.S.A*

<sup>3</sup>*Physics Department, McGill University, Montréal, Quebec, Canada, H3A 2T8*

(Dated: June 24, 2021)

We report observations of nanosecond non-uniform colloidal dynamics in a free flowing liquid jet using ultrafast x-ray speckle visibility spectroscopy. Utilizing a nanosecond double-bunch mode, the Linac Coherent Light Source free electron laser produced pairs of femtosecond coherent hard x-ray pulses. By exploring anisotropy in the visibility of summed speckle patterns which relates to the correlation functions, we evaluate not only the average particle flow rate in a colloidal nanoparticle jet, but also the non-uniform flow field within. The methodology presented here establishes the foundation for the study of nano- and atomic-scale inhomogeneous fluctuations in complex matter using x-ray free electron laser sources.

Nanoscale fluctuations of matter are closely related to transport, polarization, and mechanical properties in a wide range of materials. Dynamics in the systems under investigation often display non-uniformity, which can be intrinsic to the materials like heterogeneous dynamics concurrent with glass and jamming transitions [1] or collective avalanche-like relaxation driven by temperature, strain or magnetic and electric fields [2–4]. Studying such systems exhibiting complex non-uniform dynamical behaviors requires probes with nanoscale spatio-temporal resolution. Thermal, mechanical, or dielectric probes [5–7], as well as visible dynamic light scattering (DLS) [8], can probe the temporal behavior but lack sensitivity to nanoscale fluctuations. The x-ray analogue to DLS, x-ray photon correlation spectroscopy (XPCS), provides sensitivity on the nano and atomic length scales. However, XPCS studies have so far been limited to slow dynamics due to the relatively small scattering cross section from atomic order and the low coherent flux at current x-ray sources [9].

X-ray free electron lasers (FELs) provide new opportunities with an unprecedented high coherent flux delivered within sub-100-femtosecond pulses [10] capable of capturing snapshots freezing the atomic arrangements of the system [11]. Thus, a pair of femtosecond pulses with a time separation in the femto- to nanosecond timescales enables XPCS measurements probing fluctuations at these much faster timescales [12–17], relevant to systems with avalanche behaviors. While such timescales are beyond the current time resolution of x-ray detectors, visibility spectroscopy that relies on analyzing the contrast change of the summed speckle has been proposed,

providing information equivalent to intensity autocorrelation functions [18, 19]. Note that this approach is different from speckle visibility spectroscopy demonstrated with visible light in DLS [20] and with x-rays [21], where sample dynamics are determined by varying an integration window by modulating either detector exposure time or illumination pulse length. Following the first observation of high contrast speckle from atomic-scale order at x-ray FELs [22], much progress has been made towards applying the two-pulse modes and visibility spectroscopy to investigate homogeneous dynamics in various material systems [23–26].

In this paper, we explore nanosecond nanoscale colloidal dynamics with a non-uniformity imposed using a flowing liquid jet. The non-uniform dynamics were analyzed through the dependence of the time correlation functions on the magnitude and direction of the scattering wavevector. The methodology of probing the anisotropy of the correlation functions demonstrated here allows measuring inhomogeneous diffusion in disordered systems at previously inaccessible timescales. However, we also demonstrate that non-uniform dynamics can be unintentionally introduced, for example, as a byproduct of the sample delivery mechanisms such as within continuously flowing liquid jets or more sophisticated microfluidic devices [27, 28].

The experiment was carried out at the x-ray correlation spectroscopy instrument at the Linac Coherent Light Source [29] with the FEL operating in the so-called nanosecond double-bunch mode [12]. Pulse pairs separated by  $\tau = 49$  ns were used. The pulse pairs were attenuated by a factor of 20 to avoid beam heating and monochromatized using a 4-bounce Si(111) monochromator at 8.2 keV, with an average total pulse energy of 0.03  $\mu$ J measured at the sample plane. Beryllium compound refractive lenses  $\sim 400$  m downstream from the undulator focused the beam to  $\sim 3$   $\mu$ m at the sample with a focal length of  $\sim 3.3$  m. Slits at the lens lim-

\* Currently at Brookhaven National Laboratory, Upton, New York, 11973, USA

† Currently at MAX IV Laboratory, Lund, Sweden

‡ Send correspondence to: dlzhu@slac.stanford.edu

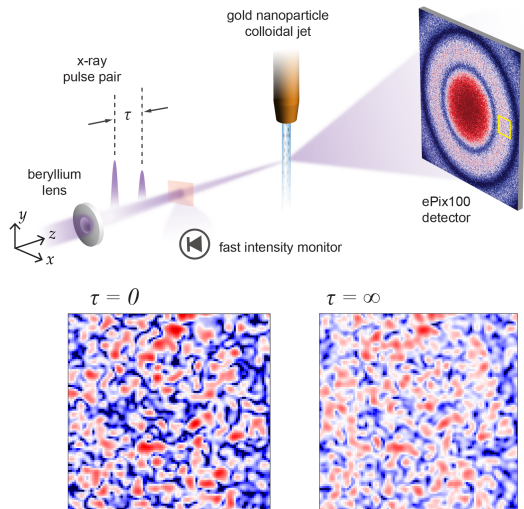


FIG. 1. Schematic of the two-pulse XPCS experiments. Two x-ray pulses with a time separation of  $\tau$  were generated using the nanosecond double-bunch mode and delivered to the sample. A high-speed intensity monitor upstream of the sample measured the relative intensities of the two pulses within each pulse pair. A 2D detector 8 meters downstream of the sample recorded the sum of the scattering from each pulse pair. Enlarged views are shown of the region of interest outlined by the yellow rectangle of the simulated speckle pattern sum for  $\tau = 0$  and  $\tau \rightarrow \infty$ , illustrating the loss of contrast when  $\tau$  exceeds the time scale of the dynamics.

ited the numerical aperture and provided a larger and more stable focal spot. Figure 1 shows the experimental schematic. The sample was a liquid water jet containing gold nanospheres of nominal  $R = 50$  nm radius (Nanopartz, 5 mg/ml,  $\Phi = 0.026$  vol%, capped with carboxylic acids for stabilization). The flow was adjustable using a Shimadzu liquid chromatography pump, and was delivered via a cylindrical glass capillary nozzle with  $d_c = 100$   $\mu\text{m}$  inner diameter. Upon exiting the nozzle, the boundary condition change led to the shrinkage of the jet known as the *vena-contracta* effect [30] and the diameter was measured to be  $d = 92$   $\mu\text{m}$  at the x-ray interaction point  $l_0 = 1.4$  mm below the nozzle using an optical microscope. A transmissive high-speed intensity monitor upstream of the sample provided a measurement of the relative intensity of the pulses within each pulse pair [31]. An ePix100 detector (pixel size, 50  $\mu\text{m}$ ,  $704 \times 768$  pixels) 8 m downstream of the sample measured the small angle scattering [32, 33], each exposure capturing the sum of x-ray scattering from a pulse pair at 120 Hz.

As proposed by Gutt, et al. [18] and Shenoy, et al. [19], the speckle contrast (the normalized variance of the intensity distribution in the speckle pattern) of the sum was obtained. This is equivalent to the intensity correlation  $g_2$  measured in sequential XPCS experiments [34, 35]. The scattering sum was recorded at flow rates between 1 to 12 mL/min, corresponding to an average speed

$\bar{v} = 2.5 - 30.1$  m/s using the jet diameter of 92  $\mu\text{m}$ . At 12 mL/min, the Reynolds number at the capillary exit was  $\approx 2876$ , at which the flow is generally considered in transition to the turbulent regime [36]. For flow rates from 1 to 8 mL/min, the flow was laminar. This agrees with observation of the jet changing from a clear gradually narrowing stream to a broadened hazy appearance at  $\approx 14$  mL/min.

Figure 2 shows the measured speckle contrast (after calibration) as a function of the flow rate for an annular region of interest (ROI) of average radius  $Q = 0.0055$   $\text{\AA}^{-1}$  and width  $\Delta Q = 0.0013$   $\text{\AA}^{-1}$  with an averaged count rate of 0.01 photons/pixel (see Fig. 4(a) in Supplemental Material). Accurate speckle contrast evaluation requires several key calibration steps. First, contrast reduction induced by sample dynamics must be separated from that due to x-ray source effects such as relative pulse pair intensity fluctuations and deviation from perfect spatial overlap. The measured contrast  $\beta$  is related to the intermediate scattering function  $f(\mathbf{Q}, \mathbf{v}, \tau)$  (where  $\mathbf{v}$  denotes the jet velocity profile) via

$$\beta = r^2\beta_1 + (1-r)^2\beta_2 + 2r(1-r)\beta_1\mu|f(\mathbf{Q}, \mathbf{v}, \tau)|^2. \quad (1)$$

Here  $\beta_1$  and  $\beta_2$  are the contrast values for each of the pulses in the pair. The pulse intensity ratio  $r \equiv i_1/(i_1 + i_2)$  varies from pulse to pulse. The parameter  $\mu$  quantifies the effective spatial overlap. An estimate of  $\mu \approx 0.74 \pm 0.02$  was obtained from analysis of scattering from a static reference sample (see Supplemental Material Section I). The second calibration step addresses systematic statistical errors of the contrast evaluation algorithms [37], where biased output of the photon assignment algorithms that are detector-response dependent can be removed. Moreover, mean intensity variation within the ROI can lead to an overestimation of the contrast [38]. Following the procedure in Supplemental Material Section II, we first grouped the scattering patterns based on  $r$ , extracted and corrected the contrasts for different  $r$  values, and subsequently fit the corrected contrasts to Eq. 1 to extract  $\beta_1$ ,  $\beta_2$  and  $|f|^2$ . We confirmed that  $\beta_1$  and  $\beta_2$  (dark/light purple in Fig. 2) agreed with each other for all flow rates within the error bars, indicating stability of the setup. The contrasts for  $r = 0.5$  were calculated and plotted as green circles in Fig. 2, where a rapid decrease was observed between 0 and 6 mL/min.

The contrast decrease can be primarily attributed to the displacement of the gold nanospheres in flow. Free diffusion, has an estimated time scale of  $\sim 70$   $\mu\text{s}$  at this  $Q$  range based on Stokes-Einstein Equation. Being much longer than the pulse separation, it can be ignored. Therefore, the intermediate scattering function at

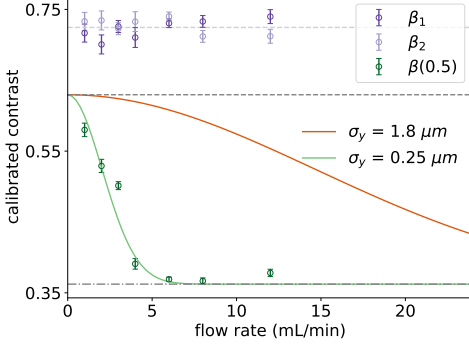


FIG. 2. Calibrated contrasts for  $r = 0, 0.5, 1$  as a function of flow rate. The curves show the calculated contrast decay assuming a uniform jet with different beam sizes. The two dashed gray lines indicate the range for  $\beta(0.5)$ . The high limit is smaller than  $\beta_{1(2)}$  due to the non-ideal spatial overlap between the two pulses.

the scattering vector  $\mathbf{Q}$  is

$$\begin{aligned} f(\mathbf{Q}, \mathbf{v}, \tau) &\approx \frac{1}{\langle N \rangle} \sum_{j=1}^{N(0)} \sum_{k=1}^{N(\tau)} \frac{\langle E_j E_k e^{i\mathbf{Q} \cdot [\mathbf{r}_k(\tau) - \mathbf{r}_j(0)]} \rangle}{\langle E_j E_k \rangle} \\ &= \frac{1}{\langle N \rangle} \sum_{j=1}^{N(0)} \frac{\langle E_j(\tau) E_j(0) e^{i\mathbf{Q} \cdot [\mathbf{r}_j(\tau) - \mathbf{r}_j(0)]} \rangle}{\langle E_j^2 \rangle}. \end{aligned} \quad (2)$$

Here the particle displacement can be approximated using the velocity field of the jet  $\mathbf{r}_j(\tau) - \mathbf{r}_j(0) = \int_0^\tau \mathbf{v} dt$ .  $E_j(\tau)$  is the electric field amplitude on the  $j$ -th gold nanoparticle at time  $\tau$ . Since the large number of particles in the scattering volume ( $\langle N \rangle \approx 3.2 \times 10^2$ ) samples the electric field over a large number of pulse pairs, the summation can be approximated as the integration over the illumination volume

$$f(\mathbf{Q}, \mathbf{v}, \tau) = \frac{\int_{V_0} E(\mathbf{r}', \tau) E(\mathbf{r}, 0) \exp(i\mathbf{Q} \cdot \mathbf{v}\tau) d\mathbf{r}}{\int_{V_0} [E(\mathbf{r}, 0)]^2 d\mathbf{r}} \quad (3)$$

Here  $\mathbf{r}$  is the location in the sample at time 0. At time  $\tau$ , the new location is at  $\mathbf{r}' = \mathbf{r} + \int_0^\tau \mathbf{v} dt \approx \mathbf{r} + \mathbf{v}\tau$ .  $E(\mathbf{r}, \tau)$  is then the electric field amplitude at time  $\tau$  for the part of the sample at location  $\mathbf{r}$  at time 0.

We first consider a uniform speed distribution, i.e., all gold particles have the same speed ( $\mathbf{v} = -\bar{v}\hat{\mathbf{y}}$ ). For a Gaussian beam spatial profile

$$E(\mathbf{r}, \tau) \approx E_0 \exp[-x^2/(2\sigma_x^2)] \exp[-(y - \bar{v}\tau)^2/(2\sigma_y^2)] \quad (4)$$

Here we neglect the  $z$ -dependence of the electric field as the sample thickness is much smaller than the Rayleigh length of the x-ray beam. See Supplemental Material Section III for more details. The intermediate scattering function reduces to

$$|f(\mathbf{Q}, \bar{v}, \tau)| = \exp\left[-\frac{(\bar{v}\tau)^2}{4\sigma_y^2}\right] \quad (5)$$

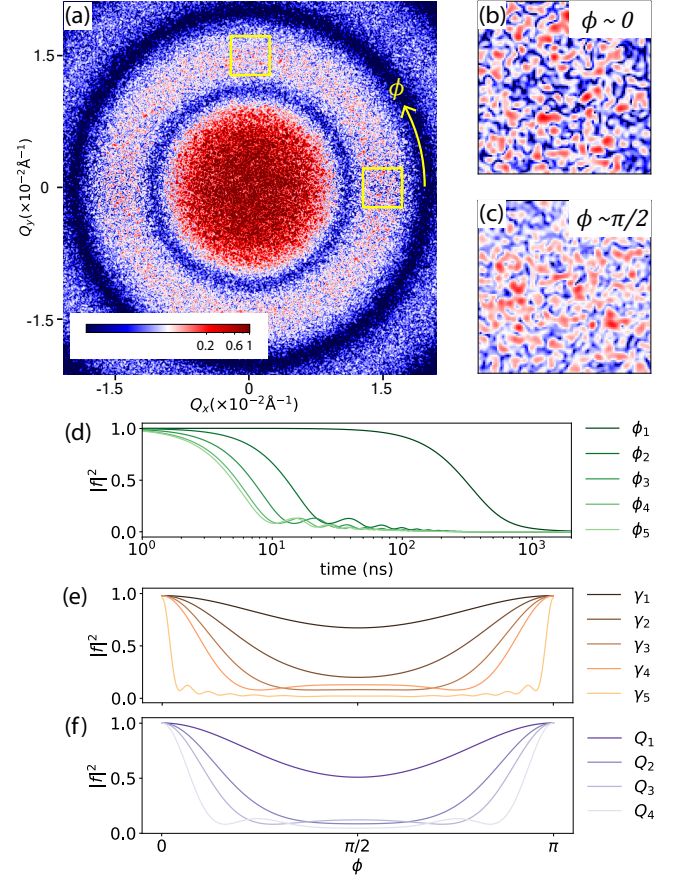


FIG. 3. Simulation of the anisotropic jet dynamics. (a) Simulated speckle pattern sum from a parabolic-flow jet at an averaged speed of  $\bar{v} = 0.5$  m/s. (b) and (c) are enlarged views of the two ROIs outlined in yellow centered at  $0.015 \text{ \AA}^{-1}$  for  $\phi \sim 0$  and  $\phi \sim \pi/2$ . (d) For fixed  $Q = 0.0055 \text{ \AA}^{-1}$ ,  $\gamma = 0$  (parabolic flow), and  $\bar{v} = 5$  m/s, calculated  $|f|^2$  as a function of time for  $\phi_{1-5} = 0, \pi/8, \pi/4, 3\pi/8$ , and  $\pi/2$ . (e) For fixed  $Q = 0.0055 \text{ \AA}^{-1}$ ,  $\bar{v} = 7.5$  m/s and  $\tau = 49$  ns, calculated  $|f|^2$  as a function of azimuthal angle  $\phi$  for  $\gamma_{1-5} = 0.95, 0.9, 0.85, 0.8$ , and  $0$ . (f) For fixed  $\bar{v} = 0.5$  m/s,  $\gamma = 0$  (parabolic flow), and  $\tau = 49$  ns, calculated  $|f|^2$  as a function of azimuthal angle  $\phi$  for  $Q_{1-4} = 0.0055, 0.011, 0.015$ , and  $0.024 \text{ \AA}^{-1}$ .

In this case the result is independent of  $\mathbf{Q}$ , since there is no spatial structure to the dynamics. A best fit (green line in Fig. 2) yields an x-ray beam size estimation of  $\sigma_y \sim 0.25 \mu\text{m}$ . This significantly deviates from  $\sigma_y \sim 1.8 \mu\text{m}$  determined from the speckle size from a static reference scattering sample. Clearly the uniform-flow model is an oversimplification of the particle dynamics within the jet at  $\tau = 49$  ns. A non-uniform-flow model is required to more accurately describe our observations [39].

We now show that the fast decay originated from the circular average over the anisotropic behavior of the decay. It is well known that when viscous liquid enters a pipe, given sufficient distance, a parabolic pipe flow profile forms. Considering the flow rate used in our ex-

periment of 1-12 mL/min, and the capillary length of  $\sim 20$  mm, this was the case. As the fluids exit the capillary, the boundary condition imposed by the wall of capillary is lifted. The radial speed difference will gradually become smaller as the center slows down and the outer part of the jet speeds up. We model the flow profile as a linear combination of the uniform and parabolic components, and use  $\gamma$  ( $0 \leq \gamma \leq 1$ ) to indicate the fraction of the uniform flow component, such that the speed field can be written as

$$v(x, z) = \gamma \bar{v} + 2(1 - \gamma) \bar{v} \left[ 1 - \frac{4(x^2 + z^2)}{d^2} \right] \quad (6)$$

The speed at the center of the jet is  $(2 - \gamma)\bar{v}$  and gradually decreases towards the boundary to  $\gamma\bar{v}$ . Considering a Gaussian beam and since  $\sigma_x/d \ll 1$ , we neglect all the  $O((\sigma_x/d)^2)$  terms. The intermediate scattering function takes the form

$$|f(\mathbf{Q}, v, \tau)| \approx \frac{1}{2} \left| \int_{-1}^1 \exp\left[i \frac{\tau}{\tau_2} 2(1 - \gamma)\zeta^2\right] \times \exp\left\{-\frac{\tau^2}{\tau_1^2} [2(1 - \gamma)(1 - \zeta^2) + \gamma]^2\right\} d\zeta \right|, \quad (7)$$

which introduces an additional timescale  $\tau_2 = [Q\bar{v} \sin \phi]^{-1}$ , with a dependence on  $\phi$  defined as the angle between  $\mathbf{Q}$  in plane and  $\hat{x}$ . The negative exponential factor dependent on  $\tau_1 = 2\sigma_y/\bar{v}$  characterizes the decrease of the intermediate scattering function due to the averaged displacement of the jet. The phase factor dependent on  $\tau_2$  modulates this amplitude. It reflects the effect of the velocity gradient within the jet. At  $\phi = 0$ , the phase factor is unity. At  $\phi = \pi/2$ , the modulation term is significant as  $\tau/\tau_2$  varies from 6.7 to 81 for flow rates 1-12 mL/min. To better illustrate the  $\phi$  dependence, we use simulated speckle patterns from particles in a parabolic flow profile (see Section IV. SPECKLE PATTERN SIMULATION in Supplemental Material), which are displayed in Fig. 3(a-c). They show the sum of scattering from two instantaneous particle positions separated in time. One can see a clear speckle visibility difference at different angular positions along a ring of constant  $|\mathbf{Q}|$ . Similar observations of the anisotropic correlation functions were reported from both DLS and XPCS studies of dynamics under continuous shear [27, 28, 40] and in the XPCS measurement of stress/strain relaxation in amorphous materials like colloidal glasses and polymers [41, 42], albeit at much slower timescales. Figure 3(f) shows  $|f|^2$  as a function of  $\phi$ , revealing a strong dependence in the vicinity of  $\phi \sim 0$  or  $\pi$ . This dependence is most prominent at small  $\gamma$  values. The timescales at  $\phi_1 = 0$  and  $\phi_5 = \pi/2$  differ by up to 2 order of magnitude as shown in Fig. 3(d). Moreover, as plotted in Fig. 3(e), one can see that  $|f(\phi)|^2$  is sensitive to  $\gamma$ , e.g., a 5% decrease from  $\gamma_1 = 0.95$  to  $\gamma_2 = 0.9$  leads to  $|f|^2$  decreasing from 0.67 to 0.20 at  $\phi = \pi/2$ .

To analyze the  $\phi$  dependence in the data, the annular ROI with average radius  $Q = 0.0055 \text{ \AA}^{-1}$  and width  $\Delta Q = 0.0013 \text{ \AA}^{-1}$  (see Fig. 4(a) in Supplemental Material) is divided into 10 sectors, each covering  $\delta\phi \approx 0.15\pi$ .

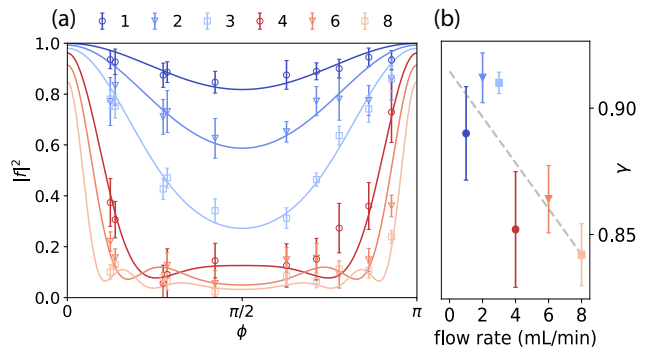


FIG. 4. (a) Dependence of  $|f|^2$  on azimuthal angle  $\phi$  for six flow rates from 1 to 8 mL/min, revealing anisotropic dynamics. The curves are fits giving the  $\gamma$  values displayed in (b). The dashed line is a guide to the eye.

The  $\phi$  value of each sector is defined using its centroid, reduced to the range of  $[0, \pi)$  assuming the equivalency between the scattering in  $\phi$  and  $\phi + \pi$ . The intensity of the intermediate scattering function is plotted for these  $\phi$  regions in the laminar flow cases with flow rates from 1 to 8 mL/min in Fig. 4(a). For each flow rate, we numerically calculated the optimal  $\gamma$  values by least squares, which is displayed in Fig. 4(b). One can see a  $\sim 5\%$  reduction in the  $\gamma$  values as the flow rate increases. This qualitatively matches the notion of the effective jet flow length  $l_e = l_0/(d_c \text{Re})$  [30], which quantifies the evolution of the velocity profile. Here Re stands for the Reynolds number.  $l_e$  is a dimensionless quantity and smaller  $l_e$  indicates earlier stage in the profile transition. With a fixed beam sample interaction location, the travel length  $l_0$  in free-flight is fixed, whereas  $l_e$  decreases as the flow rates increase giving a less uniform flow and a smaller  $\gamma$ .

Our result presents the first observation of dynamic visibility anisotropy at an x-ray FEL. We have shown that velocity profiles can be evaluated with an extended nanosecond nanoscale spatio-temporal resolution, which has many applications [39, 43–45]. From the pulse pairs in which one of them dominate in total intensity, the high contrast indicates that a single pulse ‘freezes’ the motion. Thus by using pulse pairs with shorter time separations including the nanosecond double-bunch mode or the split-delay systems [12–14, 17], one can explore the turbulent regimes. One surprising yet general implication of our result relates to the highly anticipated experiments aiming at the study of atomic-scale dynamics of supercooled liquids with the upcoming high repetition rate x-ray FELs. In order to refresh the sample for each probe pulse pair, the samples need to be delivered at high speed, either via droplets or jets. One must make sure the  $\tau_2$  equivalent of the jet delivery mechanism does not introduce dynamics on the same time scale as the intrinsic dynamics of the sample. Take a laminar water jet for example, with an average speed of 20-50 m/s,  $\tau_2$  will be in the ps time scale, e.g. at the structure factor maximum near  $2 \text{ \AA}^{-1}$ . The internal collective flow within

high speed micro droplets could be in the ps time scale as well. In such cases,  $\phi$  dependent contrast analysis will be mandatory in order to quantitatively isolate the relevant dynamics information.

Our observation also demonstrates the radial modulation of speckle contrast as a probe sensitive to the velocity gradient and thus the size of the nanoscale dynamic regions in disordered systems. By going to higher  $Q$ , the experimental observation and measurement protocol of the anisotropic nanoscale dynamics extends naturally to the atomic scale. The spatial sensitivity to nano and atomic scale non-uniformity enabled by the azimuthal dependent analysis can also be exploited together with

higher order of time correlations [46] to provide a detailed view of the heterogeneous nature of disordered systems beyond simplistic time scale analysis.

## ACKNOWLEDGMENTS

We thank Diego H. Villeneuve for helpful discussions. This work is supported by the U.S. Department of Energy, Office of Science, Office of Basic Energy Sciences under Contract No. DE-AC02-76SF00515. S.O.H. and G.B.S. supported by DOE Office of Science, Basic Energy Sciences, Division of Materials Science and Engineering.

- 
- [1] L. Berthier and G. Biroli, *Rev. Mod. Phys.* **83**, 587 (2011).
- [2] D. Fu, H. Taniguchi, M. Itoh, S.-y. Koshihara, N. Yamamoto, and S. Mori, *Phys. Rev. Lett.* **103**, 207601 (2009).
- [3] C. Sanborn, K. F. Ludwig, M. C. Rogers, and M. Sutton, *Phys. Rev. Lett.* **107**, 015702 (2011).
- [4] Z. Evenson, B. Ruta, S. Hechler, M. Stolpe, E. Pineda, I. Gallino, and R. Busch, *Phys. Rev. Lett.* **115**, 175701 (2015).
- [5] G. Wilde, *J. Non-Cryst. Solids* **312**, 537 (2002).
- [6] H. Wagner and R. Richert, *J. Chem. Phys.* **110**, 11660 (1999).
- [7] J. Qiao, J.-M. Pelletier, and R. Casalini, *J. Phys. Chem. B* **117**, 13658 (2013).
- [8] P. Ballesta, C. Ligoure, and L. Cipelletti, *AIP Conf. Proc.* **708**, 68 (2004).
- [9] O. G. Shpyrko, *J. Synchrotron Rad.* **21**, 1057 (2014).
- [10] C. Bostedt, S. Boutet, D. M. Fritz, Z. Huang, H. J. Lee, H. T. Lemke, A. Robert, W. F. Schlotter, J. J. Turner, and G. J. Williams, *Rev. Mod. Phys.* **88**, 015007 (2016).
- [11] G. B. Stephenson, A. Robert, and G. Grübel, *Nat. Mater.* **8**, 702 (2009).
- [12] F. Decker, S. Gilevich, Z. Huang, H. Loos, A. Marinelli, C. Stan, J. Turner, Z. van Hoover, and S. Vetter, *Proc. FEL2015 WEP023*, 634 (2015).
- [13] W. Roseker, H. Franz, H. Schulte-Schrepping, A. Ehnes, O. Leupold, F. Zontone, A. Robert, and G. Grübel, *Opt. Lett.* **34**, 1768 (2009).
- [14] T. Osaka, T. Hirano, Y. Sano, Y. Inubushi, S. Matsuyama, K. Tono, T. Ishikawa, K. Yamauchi, and M. Yabashi, *Opt. Express* **24**, 9187 (2016).
- [15] W. Lu, T. Noll, T. Roth, I. Agapov, G. Geloni, M. Holler, J. Hallmann, G. Ansaldi, S. Eisebitt, and A. Madsen, *AIP Conf. Proc.* **1741**, 030010 (2016).
- [16] D. Zhu, Y. Sun, D. W. Schafer, H. Shi, J. H. James, K. L. Gumerlock, T. O. Osier, R. Whitney, L. Zhang, J. Nicolas, *et al.*, *Proc. SPIE* **10237**, 102370R (2017).
- [17] Y. Sun, N. Wang, S. Song, P. Sun, M. Chollet, T. Sato, T. B. van Driel, S. Nelson, R. Plumley, J. Montana-Lopez, *et al.*, *Opt. Lett.* **44**, 2582 (2019).
- [18] C. Gutt, L.-M. Stadler, A. Duri, T. Autenrieth, O. Leupold, Y. Chushkin, and G. Grübel, *Opt. Express* **17**, 55 (2009).
- [19] G. Shenoy and J. Stoehr, *LCLS—The First Experiments*, SLAC-R-611 (SLAC National Accelerator Laboratory, Menlo Park, California, 2003).
- [20] R. Bandyopadhyay, A. Gittings, S. Suh, P. Dixon, and D. J. Durian, *Review of scientific instruments* **76**, 093110 (2005).
- [21] L. Li, P. Kwaśniewski, D. Orsi, L. Wiegart, L. Cristofolini, C. Caronna, and A. Fluerasu, *Journal of synchrotron radiation* **21**, 1288 (2014).
- [22] S. Hruszkewycz, M. Sutton, P. Fuoss, B. Adams, S. Rosenkranz, K. Ludwig Jr, W. Roseker, D. Fritz, M. Cammarata, D. Zhu, *et al.*, *Phys. Rev. Lett.* **109**, 185502 (2012).
- [23] W. Roseker, S. Hruszkewycz, F. Lehmkuhler, M. Walther, H. Schulte-Schrepping, S. Lee, T. Osaka, L. Strüder, R. Hartmann, M. Sikorski, *et al.*, *Nat. Commun.* **9**, 1704 (2018).
- [24] M. Seaberg, B. Holladay, J. Lee, M. Sikorski, A. Reid, S. Montoya, G. Dakovski, J. Koralek, G. Coslovich, S. Moeller, *et al.*, *Phys. Rev. Lett.* **119**, 067403 (2017).
- [25] V. Esposito, X. Zheng, M. Seaberg, S. Montoya, B. Holladay, A. Reid, R. Streubel, J. Lee, L. Shen, J. Koralek, *et al.*, *Appl. Phys. Lett.* **116**, 181901 (2020).
- [26] Y. Shinohara, T. Osaka, I. Inoue, T. Iwashita, W. Dmowski, C. W. Ryu, Y. Sarathchandran, and T. Egami, *Nat. Commun.* **11**, 6213 (2020).
- [27] A. Fluerasu, A. Moussaïd, P. Falus, H. Gleyzolle, and A. Madsen, *J. Synchrotron Rad.* **15**, 378 (2008).
- [28] A. Fluerasu, P. Kwasniewski, C. Caronna, F. Destremaut, J.-B. Salmon, and A. Madsen, *New J. Phys.* **12**, 035023 (2010).
- [29] R. Alonso-Mori, C. Caronna, M. Chollet, R. Curtis, D. S. Damiani, J. Defever, Y. Feng, D. L. Flath, J. M. Glowina, S. Lee, *et al.*, *J. Synchrotron Rad.* **22**, 508 (2015).
- [30] H. D. Haustein, R. S. Harnik, and W. Rohlf, *Phys. Fluids* **29**, 082105 (2017).
- [31] Y. Sun, F.-J. Decker, J. Turner, S. Song, A. Robert, and D. Zhu, *J. Synchrotron Rad.* **25**, 642 (2018).
- [32] G. Carini, R. Alonso-Mori, G. Blaj, P. Caragiulo, M. Chollet, D. Damiani, A. Dragone, Y. Feng, G. Haller, P. Hart, *et al.*, *AIP Conf. Proc.* **1741**, 040008 (2016).
- [33] M. Sikorski, Y. Feng, S. Song, D. Zhu, G. Carini, S. Herrmann, K. Nishimura, P. Hart, and A. Robert, *J. Synchrotron Rad.* **23**, 1171 (2016).
- [34] J. Carnis, W. Cha, J. Wingert, J. Kang, Z. Jiang, S. Song, M. Sikorski, A. Robert, C. Gutt, S.-W. Chen,

- et al.*, *Sci. Rep.* **4**, 6017 (2014).
- [35] F. Lehmkuhler, J. Valerio, D. Sheyfer, W. Roseker, M. A. Schroer, B. Fischer, K. Tono, M. Yabashi, T. Ishikawa, and G. Grübel, *IUCrJ* **5**, 801 (2018).
- [36] K. Avila, D. Moxey, A. de Lozar, M. Avila, D. Barkley, and B. Hof, *Science* **333**, 192 (2011).
- [37] Y. Sun, J. Montana-Lopez, P. Fuoss, M. Sutton, and D. Zhu, *J. Synchrotron Rad.* **27**, 999 (2020).
- [38] See Supplemental Material, which includes Refs. [47, 48].
- [39] J. R. Lhermitte, M. C. Rogers, S. Manet, and M. Sutton, *Rev. Sci. Instrum.* **88**, 015112 (2017).
- [40] B. Ackerson and N. Clark, *J. phys.* **42**, 929 (1981).
- [41] F. Dallari, A. Martinelli, F. Caporaletti, M. Sprung, G. Grübel, and G. Monaco, *Sci. Adv.* **6**, eaaz2982 (2020).
- [42] M. Sutton, J. R. Lhermitte, F. Ehrburger-Dolle, and F. Livet, *Phys. Rev. Res.* **3**, 013119 (2021).
- [43] G. Fuller, J. Rallison, R. Schmidt, and L. Leal, *J. Fluid Mech.* **100**, 555 (1980).
- [44] T. Narayanan, C. Cheung, P. Tong, W. I. Goldberg, and X.-l. Wu, *Appl. Opt.* **36**, 7639 (1997).
- [45] F. Lehmkuhler, I. Steinke, M. A. Schroer, B. Fischer, M. Sprung, and G. Grbel, *The journal of physical chemistry letters* **8**, 3581 (2017).
- [46] A. Madsen, R. L. Leheny, H. Guo, M. Sprung, and O. Czakkel, *New J. Phys.* **12**, 055001 (2010).
- [47] A. Sandy, L. Lurio, S. Mochrie, A. Malik, G. Stephenson, J. Pelletier, and M. Sutton, *J. Synchrotron Rad.* **6**, 1174 (1999).
- [48] M. Sikorski, S. Song, A. Schropp, F. Seiboth, Y. Feng, R. Alonso-Mori, M. Chollet, H. T. Lemke, D. Sokaras, T.-C. Weng, *et al.*, *J. Synchrotron Rad.* **22**, 599 (2015).